

# $g$ -factor and static quadrupole moment of $^{135}\text{Pr}$ , $^{105}\text{Pd}$ , and $^{187}\text{Au}$ in wobbling motion

C. Broocks,<sup>1</sup> Q. B. Chen,<sup>2,1,\*</sup> N. Kaiser,<sup>1,†</sup> and Ulf-G. Meißner<sup>3,4,‡</sup>

<sup>1</sup>Physik-Department, Technische Universität München, D-85747 Garching, Germany

<sup>2</sup>Department of Physics, East China Normal University, Shanghai 200241, China

<sup>3</sup>Helmholtz-Institut für Strahlen- und Kernphysik and Bethe Center for Theoretical Physics, Universität Bonn, D-53115 Bonn, Germany

<sup>4</sup>Institute for Advanced Simulation, Institut für Kernphysik, Jülich Center for Hadron Physics and JARA-HPC, Forschungszentrum Jülich, D-52425 Jülich, Germany

(Dated: March 25, 2021)

The  $g$ -factor and static quadrupole moment of the nuclides  $^{135}\text{Pr}$ ,  $^{105}\text{Pd}$ , and  $^{187}\text{Au}$  in the wobbling motion are investigated in the particle-rotor model as functions of the total spin  $I$ . The  $g$ -factor of  $^{105}\text{Pd}$  increases with increasing  $I$ , due to the negative gyromagnetic ratio of a neutron valence-neutron. This behavior is in contrast to the decreasing  $g$ -factor of the other two nuclides,  $^{135}\text{Pr}$  and  $^{187}\text{Au}$ , which feature a valence-proton. The static quadrupole moment  $Q$  depends on all three expectation values of the total angular momentum. It is smaller in the yrast band than in the wobbling band for the transverse wobblers  $^{135}\text{Pr}$  and  $^{105}\text{Pd}$ , while larger for the longitudinal wobblers  $^{187}\text{Au}$ .

The collective wobbling motion of nuclei, as proposed long ago by Bohr and Mottelson [1], is a direct evidence for the existence of nuclides with triaxially deformed shape. Such a triaxially deformed nucleus rotates about the principal axis associated to the largest moment of inertia and this axis executes harmonic oscillations about the space-fixed total angular momentum vector. The energy spectra related to this collective wobbling motion consist of a series of rotational bands corresponding to increasing excitations ( $n$ ) of harmonic oscillation quanta. The transitions between the rotational bands with  $\Delta I = 1$  have a dominant electric quadrupole ( $E2$ ) character.

For the wobbling modes in the presence of a high- $j$  valence-nucleon, Frauendorf and Dönau introduced the concepts of *transverse* wobbling (TW) and *longitudinal* wobbling (LW) [2]. This classification is based on the relative orientation of the angular momentum of the valence-particle  $\mathbf{j}_p$  and the principal axis associated to the largest moment of inertia (usually the intermediate axis). Transverse wobbling means that this relative orientation is perpendicular, while for longitudinal wobbling it is parallel. The excitation energy of the wobbling mode with  $n = 1$  (also called wobbling energy) in a transverse (longitudinal) wobblers decreases (increases) with total spin  $I$  [2].

Experimental data for wobbling bands in odd-mass nuclei are available for the nuclides  $^{187}\text{Au}$  [3] and  $^{183}\text{Au}$  [4] in the  $A \approx 190$  mass region, for  $^{161}\text{Lu}$  [5],  $^{163}\text{Lu}$  [6, 7],  $^{165}\text{Lu}$  [8],  $^{167}\text{Lu}$  [9], and  $^{167}\text{Ta}$  [10] in the  $A \approx 160$  mass region, for  $^{135}\text{Pr}$  [11, 12],  $^{133}\text{La}$  [13],  $^{130}\text{Ba}$  [14, 15], and  $^{127}\text{Xe}$  [16] with mass number  $A \approx 130$ , and moreover for

$^{105}\text{Pd}$  [17] in the  $A \approx 100$  mass region. Among these,  $^{133}\text{La}$ ,  $^{187}\text{Au}$ , and  $^{127}\text{Xe}$  were interpreted as longitudinal wobblers, while the others are regarded as transverse wobblers.

It should be noted that almost all experiments focus on energy spectra and electromagnetic transition probabilities, while nuclear multipole moments are studied very rarely. The  $g$ -factor and static quadrupole moment (SQM) have been measured only for the bandhead state in  $^{133}\text{La}$  [18] and their behavior as a function of spin  $I$  were predicted in Ref. [19] employing the particle-rotor model (PRM). At the same time the dependences of the  $g$ -factor and SQM on the spin  $I$  have been interpreted in detail by analyzing the angular momentum components of the rotor, proton-particle, and total nuclear system with the help of various quantum-mechanical probability distributions. This study has shown that the  $g$ -factor and SQM are good indicators of the angular momentum geometry underlying a triaxially deformed nucleus in the collective wobbling motion.

Motivated by these achievements, we will study in the present work the  $g$ -factor and SQM for the nuclides  $^{135}\text{Pr}$ ,  $^{105}\text{Pd}$ , and  $^{187}\text{Au}$  in the collective wobbling mode. The reason for choosing these three nuclei are that they lie in different mass regions, and that  $^{135}\text{Pr}$  and  $^{187}\text{Au}$  show the typical TW and LW modes, respectively. Moreover,  $^{105}\text{Pd}$  is the first wobbling nucleus with an odd neutron number.

Following Ref. [19], our present calculations are carried out within the PRM, which has been used widely and successfully for describing wobbling bands [2, 15, 20–27]. The formulas for calculating the  $g$ -factor and SQM in PRM can be found in Refs. [19, 28], but for completeness we give a brief introduction into the formalism.

The  $g$ -factor is of particular interest, because its value depends crucially on the alignment of the involved angular momenta, and moreover it is an experimentally measurable quantity. The  $g$ -factor connects the total spin

\*Electronic address: qbchen@pku.edu.cn

†Electronic address: nkaiser@ph.tum.de

‡Electronic address: meissner@hiskp.uni-bonn.de

quantum number  $I$  with the expectation value of the magnetic moment  $\mu$  and it can be calculated with the help of the generalized Landé formula as:

$$\mu = g(I)I = \frac{\langle II | g_p \mathbf{j} \cdot \mathbf{I} + g_R \mathbf{R} \cdot \mathbf{I} | II \rangle}{I(I+1)}. \quad (1)$$

The wave function  $|II\rangle$  refers to  $|I, M=I\rangle$  with  $M$  the quantum number related to the projection of  $\mathbf{I}$  onto the  $z$ -axis in the laboratory frame. The parameters  $g_p$  and  $g_R$  are the gyromagnetic ratios of the valence-nucleon (with angular momentum operator  $\mathbf{j}$ ) and the collective rotor (with angular momentum operator  $\mathbf{R}$ ). Using the relation  $\mathbf{R} = \mathbf{I} - \mathbf{j}$  one can import into the Landé formula some information about the alignment of the involved angular momenta,

$$g(I) = \frac{\langle II | g_p \mathbf{j} \cdot \mathbf{I} + g_R \mathbf{R} \cdot \mathbf{I} | II \rangle}{I(I+1)} \quad (2)$$

$$= g_R + (g_p - g_R) \frac{\langle \mathbf{j} \cdot \mathbf{I} \rangle}{I(I+1)} \quad (3)$$

$$= g_R + (g_p - g_R) \frac{j(j+1)}{I(I+1)} + (g_p - g_R) \frac{\langle \mathbf{j} \cdot \mathbf{R} \rangle}{I(I+1)}. \quad (4)$$

where  $\mathbf{I} = \mathbf{R} + \mathbf{j}$  has been applied in the last step. On the other hand, replacing  $\mathbf{j}$  by  $\mathbf{I} - \mathbf{R}$  in Eq. (2) gives

$$g(I) = g_p + (g_R - g_p) \frac{\langle \mathbf{R} \cdot \mathbf{I} \rangle}{I(I+1)}. \quad (5)$$

Combining Eqs. (4) and (5) yields an expression for  $g(I)$  that depends only on the quantum numbers  $I, j$ , and the expectation value of the squared rotor angular momentum  $\mathbf{R}^2$ ,

$$g(I) = \frac{1}{2} \left[ (g_p + g_R) + (g_p - g_R) \frac{j(j+1) - \langle \mathbf{R}^2 \rangle}{I(I+1)} \right]. \quad (6)$$

If one measures  $g(I)$  with its  $I$ -dependence and knows  $j$ , which is the case for a given nucleus, this formula provides direct information about the expectation values of  $\mathbf{R}^2$ . In the case of perpendicular or parallel alignment of the angular momenta, simpler expressions for the  $g$ -factor are obtained [19]:

$$g(I) = g_p, \quad \text{for } \mathbf{R} \perp \mathbf{I}; \quad (7)$$

$$= g_R, \quad \text{for } \mathbf{j} \perp \mathbf{I}; \quad (8)$$

$$= g_R + (g_p - g_R) \frac{j(j+1)}{I(I+1)}, \quad \text{for } \mathbf{j} \perp \mathbf{R}; \quad (9)$$

$$= g_R + (g_p - g_R) \sqrt{\frac{j(j+1)}{I(I+1)}}, \quad \text{for } \mathbf{j} \parallel \mathbf{I}. \quad (10)$$

The other measurable quantity that encodes some information about the angular momentum geometry is the static quadrupole moment (SQM). It provides a measure of the non-sphericity of the nuclear charge distribution and can be calculated as the diagonal matrix-element

$$Q(I) = \langle II | \hat{Q}_{20} | II \rangle, \quad (11)$$

where the quadrupole moment operator  $\hat{Q}_{20}$  in the laboratory frame is obtained from the intrinsic quadrupole moments  $Q'_{2\nu}$  by multiplication with Wigner  $D$ -functions:

$$\hat{Q}_{20} = \sum_{\nu=-2}^2 D_{0,\nu}^2 Q'_{2\nu}. \quad (12)$$

The five intrinsic quadrupole moments are  $Q'_{20} = Q'_0 \cos \gamma$ ,  $Q'_{21} = Q'_{2-1} = 0$ , and  $Q'_{22} = Q'_{2-2} = Q'_0 \sin \gamma / \sqrt{2}$ , where  $Q'_0$  is an empirical quadrupole moment that is related to the axial deformation parameter  $\beta$  by  $Q'_0 = 3R_0^2 Z \beta / \sqrt{5\pi}$ , with  $Z$  the proton number and  $R_0 = 1.2 \text{ fm } A^{1/3}$ .

One possibility to calculate the SQM is to use the expectation value of the squared total angular momentum components along the three principal axes  $\langle \hat{I}_k^2 \rangle$  [19, 28],

$$Q(I) = Q_0(I) + Q_2(I), \quad (13)$$

$$Q_0(I) = \frac{3\langle \hat{I}_3^2 \rangle - I(I+1)}{(I+1)(2I+3)} Q'_0 \cos \gamma, \quad (14)$$

$$Q_2(I) = \frac{\sqrt{3}(\langle \hat{I}_1^2 \rangle - \langle \hat{I}_2^2 \rangle)}{(I+1)(2I+3)} Q'_0 \sin \gamma. \quad (15)$$

This form has the advantage that one can get some information about the spin orientation from  $Q(I)$ .

For the nuclides  $^{135}\text{Pr}$  [11, 12],  $^{105}\text{Pd}$  [17], and  $^{187}\text{Au}$  [3], the PRM has been used to reproduce the experimental energy spectra and wobbling energies together with the electromagnetic transition probability ratios,  $B(M1)_{\text{out}}/B(E2)_{\text{in}}$  and  $B(E2)_{\text{out}}/B(E2)_{\text{in}}$  for their wobbling bands. In this work, we focus on the  $g$ -factor and SQM. The pertinent numerical details, including the deformation parameters, moments of inertia,  $g$ -factors of valence-nucleon and rotor, and empirical quadrupole moments, can be found in Refs. [3, 11, 12, 17].

We will first discuss the results for the  $g$ -factor of these three wobbling nuclei. The calculated values of  $g(I)$  are shown in Fig. 1. For  $^{135}\text{Pr}$  (see Fig. 1(a)) the  $g$ -factor decreases with increasing  $I$  down to a value  $g(I=15.5) = 0.7$  and this decrease is faster for small  $I$ -values. The results for  $^{187}\text{Au}$  displayed in Fig. 1(c) show the same trend with  $g(I=4.5) = 0.75$  at the bandhead and a decrease down to  $g(I=18.5) = 0.5$ . However, the  $g$ -factor of  $^{105}\text{Pd}$  (see Fig. 1(b)) shows an inverted behavior with an increasing  $g$ -factor from  $g(I=5.5) = -0.2$  at the bandhead up to  $g(I=15.5) = 0.2$  at the highest calculated  $I$ -value.

One can explain the behavior of the  $g$ -factor shown in Fig. 1 by considering its dependence on the gyromagnetic ratios  $g_p$  and  $g_R$ , the quantum numbers  $j$  and  $I$ , and the expectation value of the rotor angular momentum  $\sqrt{\langle \mathbf{R}^2 \rangle}$ , as written in Eq. (6). For this purpose we show in Fig. 2 the expectation value of the rotor angular momentum  $\bar{R} = \sqrt{\langle \mathbf{R}^2 \rangle} = \sqrt{\langle R_s^2 \rangle + \langle R_m^2 \rangle + \langle R_l^2 \rangle}$ . A comparison of these plots for the three nuclei reveals that  $^{135}\text{Pr}$  and  $^{105}\text{Pd}$  feature very similar  $\bar{R}$ -values. For

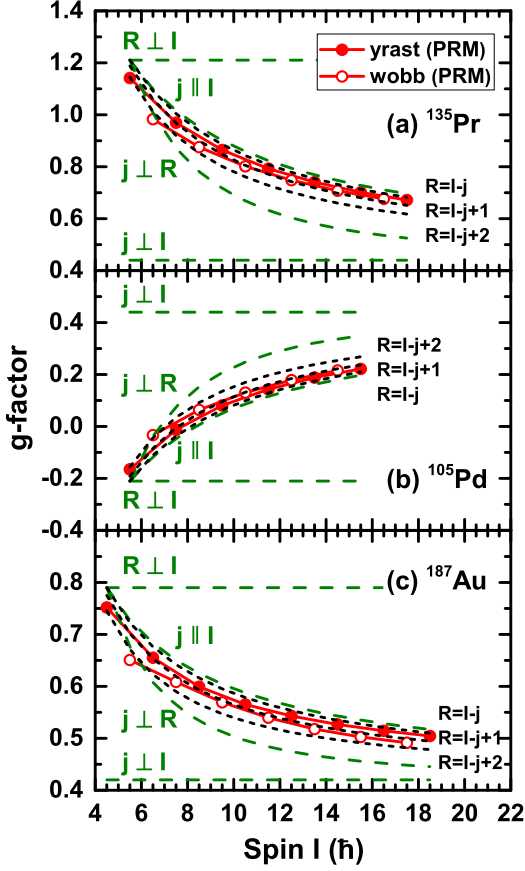


FIG. 1: PRM calculation of the  $g$ -factor in the yrast and wobbling band for the nuclei  $^{135}\text{Pr}$  (a),  $^{105}\text{Pd}$  (b), and  $^{187}\text{Au}$  (c). The dashed lines for special alignment cases  $\mathbf{R} \perp \mathbf{I}$ ,  $\mathbf{j} \perp \mathbf{I}$ ,  $\mathbf{j} \perp \mathbf{R}$ , and  $\mathbf{j} \parallel \mathbf{I}$  are calculated with Eqs. (7)-(10). The dotted curves show the trend of the  $g$ -factor, approximating the rotor angular momentum by  $\langle \mathbf{R}^2 \rangle = R(R+1)$  with  $R = I - j$ ,  $R = I - j + 1$  or  $R = I - j + 2$ , and using Eq. (6).

small values of spin  $I$ , the  $\bar{R}$ -values in the wobbling band are larger than in the yrast band, but with increasing  $I$ , this difference becomes smaller. One observes that  $\bar{R}$  increases almost linearly from  $\bar{R}(I = 5.5) = 2$  in the yrast band and  $\bar{R}(I = 6.5) = 4$  in the wobbling band up to a similar value of  $\bar{R}(I = 18.5) = 15$ . The values for  $^{187}\text{Au}$  are slightly higher. While  $j$  is constant for each nucleus, one observes that  $\bar{R}$  increases with growing  $I$ .

In order to explain the decreasing and increasing  $g$ -factors, we take a closer look at both parts in Eq. (6). The constant offset  $(g_p + g_R)/2$  is 0.8 for  $^{135}\text{Pr}$  and 0.6 for  $^{187}\text{Au}$ , but has a much smaller value of 0.1 for  $^{105}\text{Pd}$ . The second part in the  $g$ -factor formula is of the form:  $(g_p - g_R)[j(j+1) - \langle \mathbf{R}^2 \rangle] / [2I(I+1)]$ . For the nuclei with  $j = 5.5$  ( $^{135}\text{Pr}$  and  $^{105}\text{Pd}$ ),  $\bar{R}$  is smaller than  $\bar{j} = \sqrt{j(j+1)} \approx 6.0$  up to  $I = 9.5$ . For  $^{187}\text{Au}$  with  $j = 4.5$ ,  $\bar{R}$  is smaller than  $\bar{j} \approx 5.0$  up to  $I = 7.5$ . Therefore, the difference is positive for small  $I$  and it becomes smaller or even negative with increasing  $I$ . Since the coefficient  $g_p - g_R$  is positive for  $^{135}\text{Pr}$  and  $^{187}\text{Au}$ , the  $g$ -factors of these two

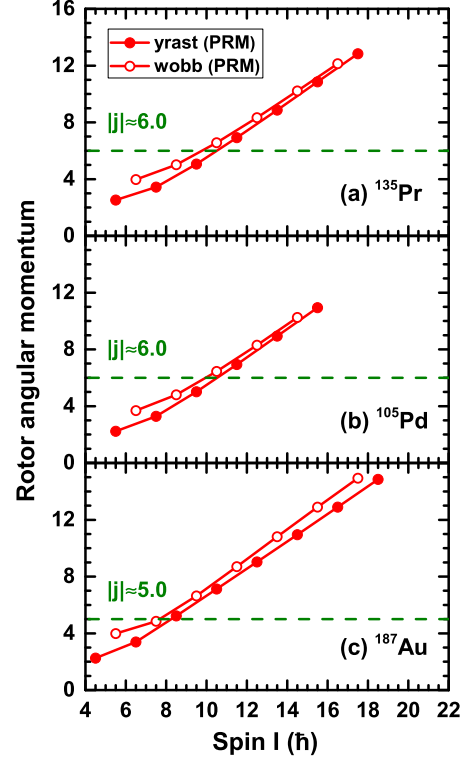


FIG. 2: The square root of the expectation value of the squared rotor angular momentum  $\bar{R} = \langle \mathbf{R}^2 \rangle^{1/2}$  for states in the yrast and wobbling bands of  $^{135}\text{Pr}$ ,  $^{105}\text{Pd}$ , and  $^{187}\text{Au}$ . The horizontal line in each plot corresponds to the length of the particle angular momentum  $\bar{j} \approx j + 0.5$ . It delineates the region of low spins  $I$ , where the particle angular momentum is larger than the rotor angular momentum.

nuclei are bigger than the constant  $(g_p + g_R)/2$  at the bandhead and they decrease with increasing  $I$ . Because of the valence-neutron in  $^{105}\text{Pd}$ ,  $g_p - g_R$  is negative and the second piece is negative for small  $I$  and positive for  $I > 9.5$ . This explains the increasing  $g$ -factor of this nucleus. In the limit of very high  $I$ , the rotor angular momentum tends to  $\langle \mathbf{R}^2 \rangle \rightarrow I(I+1)$  and  $j$  becomes negligible  $j(j+1) \ll \langle \mathbf{R}^2 \rangle$ . In this case the  $g$ -factor approaches the value  $g_R$ .

Since  $g_p$  and  $g_R$  are measurable,  $\langle \mathbf{R}^2 \rangle$  is the only unknown in Eq. (6) and can therefore be extracted from the experimental  $g$ -factor for each single spin-state  $I$ . Nevertheless, it can be helpful to compare the measured  $g$ -factors with a model calculation when  $\langle \mathbf{R}^2 \rangle$  is significant in order to see tendencies and to do a consistency checks. For this reason we insert in Fig. 1 three dotted lines that give the  $g$ -factor obtained with rotor angular momentum quantum numbers  $R = I - j$ ,  $R = I - j + 1$ , and  $R = I - j + 2$  using the relation  $\langle \mathbf{R}^2 \rangle = R(R+1)$ . Since all three nuclei have very similar values of  $\langle \mathbf{R}^2 \rangle$ , the calculated  $g$ -factors tend to the same lines of approximation. At the bandhead the  $g$ -factor of the yrast state is close to the  $R = I - j + 2$  line, where the rotor angular momentum is approximated by  $\sqrt{R(R+1)} = 2.44$ . For large

values of  $I$ , the  $g$ -factors of yrast and wobbling states are in better agreement with the curves for  $R = I - j$  and  $R = I - j + 1$ , respectively. The slightly larger ( $R^2$ )-values for  $^{187}\text{Au}$  favor the  $R = I - j + 2$  curve for the  $g$ -factors of wobbling states.

The third set of curves displayed in Fig. 1 are the dashed lines corresponding to specific alignment situations  $\mathbf{R} \perp \mathbf{I}$ ,  $\mathbf{j} \perp \mathbf{I}$ ,  $\mathbf{j} \perp \mathbf{R}$ , and  $\mathbf{j} \parallel \mathbf{I}$ . For small  $I$  in the yrast band, the calculated  $g$ -factor is close to any of the  $\mathbf{R} \perp \mathbf{I}$ ,  $\mathbf{j} \perp \mathbf{R}$ , and  $\mathbf{j} \parallel \mathbf{I}$  curves. These curves intersect at the bandhead since Eqs. (7), (9), and (10) give there the same value  $g = g_p$ .

For higher spin  $I$ , the calculated  $g$ -factors for all three nuclei lie between the  $\mathbf{j} \parallel \mathbf{I}$  and the  $\mathbf{j} \perp \mathbf{R}$  curves, tending towards  $\mathbf{j} \parallel \mathbf{I}$  for increasing  $I$ . The  $g$ -factors in yrast states are always closer to the parallel-alignment curve than those in wobbling states. This is plausible, since  $\mathbf{I}$  in a wobbling state is tilted further away from  $\mathbf{j}$  than in the respective yrast case. For the first wobbling band this implies that  $\mathbf{R}$  has a better agreement with perpendicular alignment to  $\mathbf{j}$  than in the case of the yrast band. The increasing agreement for both bands with the  $\mathbf{j} \parallel \mathbf{I}$  curve is a clue for the change from a transverse to a longitudinal alignment of the particle angular momentum.

Next, we present in Fig. 3 the SQM results for the three nuclei, based on Eq. (13). In the calculation, we replace the triaxial deformation parameter  $\gamma$  by  $\gamma + 240^\circ$  which corresponds to the same shape, but then  $Q_0$  vanishes almost due the smallness of  $\cos(\gamma + 240^\circ) = -0.087$  with  $\gamma \sim 25^\circ$  for the three nuclei [3, 11, 12, 17]. This setup provides a more promising chance to gain information about the angular momentum components from the second contribution  $Q_2(I)$ . Note that according to this choice the assignment of principal axes is: 1  $\rightarrow$   $s$ , 2  $\rightarrow$   $l$ , and 3  $\rightarrow$   $m$ . The individual contributions  $Q_0(I)$  and  $Q_2(I)$  to  $Q(I)$  are displayed in Fig. 3 by dashed and dotted lines, respectively.

A first observation is that the SQM is negative for all three nuclei and every calculated  $I$ -value, which is attributed to a much smaller angular momentum component of the  $l$ -axis compared to the  $s$ -axis.

Fig. 3(a) shows that the SQM of  $^{135}\text{Pr}$  changes from decreasing to increasing at  $I = 9.5$  in the yrast band and a similar trend is indicated at  $I = 12.5$  in the wobbling band. However, the change of the SQM in the wobbling band is not very pronounced and it appears to be almost constant for high spins. The difference between the SQMs in the yrast and wobbling band decreases with increasing  $I$ , and the two curves cross almost at  $Q(I = 16.5) = -1.1$  eb. The contribution  $Q_0(I)$  has a minor tendency towards negative values, but in comparison to  $Q_2(I)$  it can be approximated by  $Q_0(I) = 0$ . With respect to the SQMs the nucleus  $^{105}\text{Pd}$  shown in Fig. 3(b) exhibits a behavior very similar to  $^{135}\text{Pr}$ . At the value  $Q(I = 14.5) = -1.15$  eb, the SQM in the yrast band becomes larger than that in the wobbling band. Note that both nuclides were interpreted as transverse wobblers at the low spins [11, 12, 17]. At higher spins, a transition

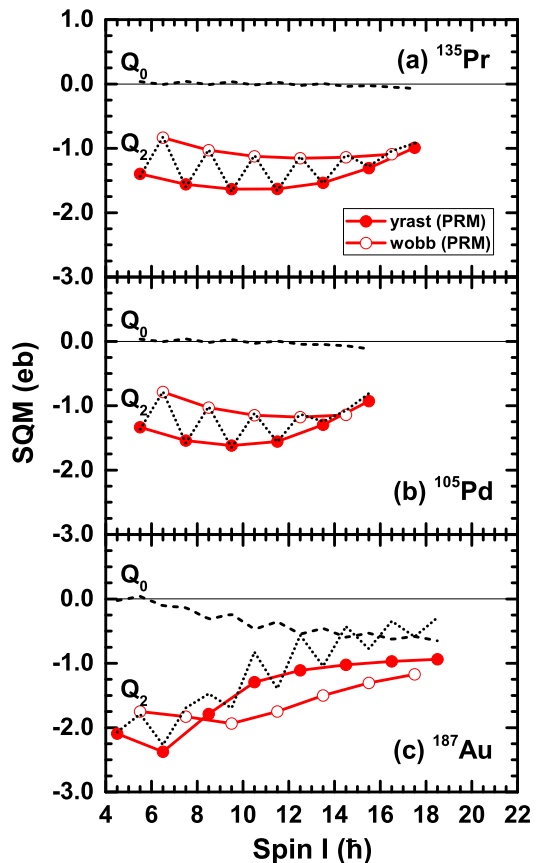


FIG. 3: Static quadrupole moments for states in the yrast and wobbling bands of the nuclei  $^{135}\text{Pr}$ (a),  $^{105}\text{Pd}$  (b) and  $^{187}\text{Au}$  (c). The contributions  $Q_0$  and  $Q_2$  are calculated with Eqs. (14) and (15) using the choice  $\gamma \rightarrow \gamma + 240^\circ$ .

to longitudinal wobbling can happen (e.g., in  $^{135}\text{Pr}$  [11] for  $I \geq 14.5$ ). Hence the crossing of SQM curves of yrast and wobbling bands indicates the transverse wobbling collapses.

In Fig. 3(c) a slightly different behavior can be seen for the nuclide  $^{187}\text{Au}$ , which according to Ref. [3] supports the picture of a longitudinal wobbler. For states in the yrast band the SQM starts from  $Q(I = 4.5) = -2.1$  eb, decreases to  $Q(I = 6.5) = -2.4$  eb, and then develops a declining increase up to  $Q(I = 18.5) = -1.0$  eb. The SQM of states in the wobbling band first decreases from  $Q(I = 5.5) = -1.75$  eb to  $Q(I = 9.5) = -2.0$  eb, and beyond that its value increases almost linearly up to  $Q(I = 17.5) = -1.17$  eb. The difference between SQM-values for states in the yrast and wobbling band decreases again at high spin  $I$ . Whereas  $Q_0(I)$  vanishes for the low spins, it becomes even larger in magnitude than  $Q_2(I)$  at the higher spins. This is caused by the longitudinal wobbling motion, in which the total angular momentum, as shown in the following, aligns along the  $m$ -axis.

For  $^{135}\text{Pr}$  and  $^{105}\text{Pd}$  the behavior of the SQM follows from the expression  $Q_2(I)$  in Eq. (14), since  $\cos \gamma$  is close to zero and/or  $3\langle \hat{I}_m^2 \rangle \approx I(I+1)$ . To check the last condi-



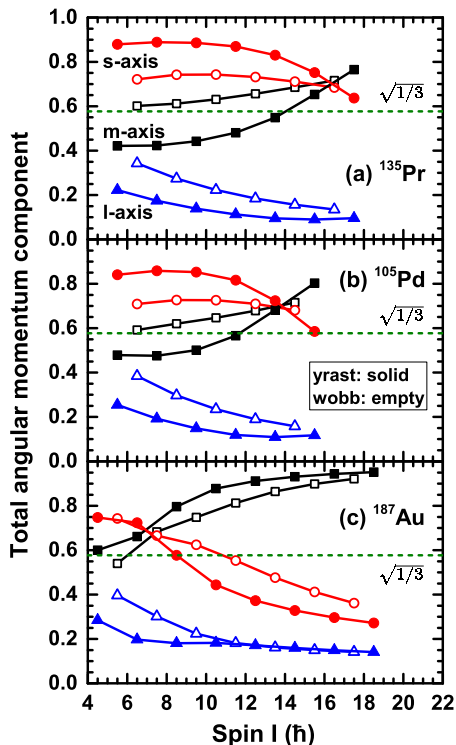


FIG. 4: Ratio-plots  $r_k = \sqrt{\langle \hat{I}_k^2 \rangle} / \sqrt{I(I+1)}$  of the total angular momentum components along the short ( $s$ -), intermediate ( $m$ -), and long ( $l$ -) axes for states in the yrast and wobbling bands of  $^{135}\text{Pr}$ ,  $^{105}\text{Pd}$ , and  $^{187}\text{Au}$ .

tion and to show the behavior of individual total angular momentum components, ratio-plots

$$r_k = \frac{I_k}{\sqrt{I_s^2 + I_m^2 + I_l^2}} = \frac{\sqrt{\langle \hat{I}_k^2 \rangle}}{\sqrt{I(I+1)}} \quad (16)$$

of the total angular momentum components along the short ( $s$ -), intermediate ( $m$ -), and long ( $l$ -) axes with respect to the length of the total spin are presented in Fig. 4. The dotted horizontal line at height  $\sqrt{1/3}$  corresponds to the situation  $3\langle \hat{I}_m^2 \rangle = I(I+1)$ .

There is good agreement between  $r_m$  and  $\sqrt{1/3}$  for states in the wobbling band of  $^{135}\text{Pr}$  and  $^{105}\text{Pd}$  at low spins  $I$ , as can be seen in Fig. 4. The decreasing SQM for small  $I$  is caused by the denominator  $(I+1)(2I+3)$ , whereas for higher  $I$  the numerator  $\sqrt{3}(\langle \hat{I}_s^2 \rangle - \langle \hat{I}_l^2 \rangle)$  is increasing faster. The  $l$ -component  $I_l$  is almost constant with  $I_l \approx 1.5$  for states in the yrast band and  $I_l \approx 2.5$  for states in the wobbling band. The  $s$ -component  $I_s$  is larger for states in the yrast band than in the wobbling band and it increase with  $I$ . This is the reason, why the SQM difference is positive and has larger values in yrast band than in the wobbling band. The SQM is always negative due to the negative prefactor  $\sin(\gamma+240^\circ)$ . The nuclides  $^{135}\text{Pr}$  and  $^{105}\text{Pd}$  show the same tendency.

For  $^{187}\text{Au}$ , the absolute value of the SQM of the yrast states becomes smaller than that in the wobbling states

for larger  $I$ , because  $I_s$  of the yrast states gets smaller than  $I_s$  of the wobbling states. This is a feature of a longitudinal wobblers with respect to the  $m$ -axis.

To explain the behavior of the SQM for  $^{187}\text{Au}$  more detailed, one needs to consider the  $Q_2(I)$ -part of  $Q(I)$ , because  $r_m$  becomes significantly larger than  $\sqrt{1/3}$ , in particular in the high spin region. The  $I_m$ -values for states in the wobbling and the yrast band are not very different from each other and the increasing negative value of  $Q_0(I)$  is responsible for the difference between  $Q_2(I)$  and the full SQM. At high spins the contributions  $Q_0(I)$  and  $Q_2(I)$  are almost equal for large values of  $I$ . The difference of the SQM between states in the wobbling and yrast band becomes smaller, because  $I_s$  and  $I_l$  are almost constant for the longitudinal alignment at high  $I$ -values and the denominator  $(I+1)(2I+3)$  causes the values in both bands to be small and close to each other. At the same time  $Q_0$  is responsible for the fact that the absolute value of the SQM is not decreasing. For very high  $I$ -values, one expects that due to the longitudinal alignment  $I_m$  is dominant and approximately as big as  $I$ , such that  $Q_2(I)$  vanishes and  $Q_0(I)$  tends to  $Q'_0 \cos \gamma$ .

In summary, the  $g$ -factor and static quadrupole moment (SQM) for the wobbling mode of  $^{135}\text{Pr}$ ,  $^{105}\text{Pd}$ , and  $^{187}\text{Au}$  have been investigated in the framework of the PRM. The  $g$ -factor allows one to deduce the expectation value of the rotor angular momentum  $\bar{R}$ . Due to the negative gyromagnetic ratio of a valence-neutron, the  $g$ -factor of  $^{105}\text{Pd}$  is increasing with increasing spin  $I$ , in contrast to the decreasing  $g$ -factor of the other two nuclides  $^{135}\text{Pr}$  and  $^{187}\text{Au}$  with a valence-proton. The SQM depends on all three total angular momentum component expectation values  $I_s$ ,  $I_m$ , and  $I_l$ . It is smaller in yrast band than in wobbling band for the transverse wobblers  $^{135}\text{Pr}$  and  $^{105}\text{Pd}$ , while larger for the longitudinal wobblers  $^{187}\text{Au}$ .

At present, there are no experimental data for the  $g$ -factor and SQM of these three nuclei ( $^{135}\text{Pr}$ ,  $^{105}\text{Pd}$ , and  $^{187}\text{Au}$ ). Therefore, we could only outline which information one can extract from these observable and explain the tendencies of these quantities in the PRM. Future experimental efforts along this direction are of high importance. Moreover, theoretical investigations for  $g$ -factor and SQM using more sophisticated methods, such as random phase approximation based on cranking approach [29–32], collective Hamiltonian based on tilted axis cranking approach [33, 34], or triaxial projected shell model [35–37], will be interesting also.

## Acknowledgements

Financial support for this work was provided in parts by Deutsche Forschungsgemeinschaft (DFG) and National Natural Science Foundation of China (NSFC) through funds provided to the Sino-German CRC 110 ‘‘Symmetries and the Emergence of Structure in QCD’’ (DFG Project-ID 196253076, NSFC Grant

No. 12070131001). The work of UGM was also supported by the Chinese Academy of Sciences (CAS) through a President's International Fellowship Initiative

(PIFI) (Grant No. 2018DM0034) and by the Volkswagen Stiftung (Grant No. 93562).

- 
- [1] A. Bohr and B. R. Mottelson, *Nuclear structure*, vol. II (Benjamin, New York, 1975).
- [2] S. Frauendorf and F. Dönau, *Phys. Rev. C* **89**, 014322 (2014).
- [3] N. Sensharma, U. Garg, Q. B. Chen, S. Frauendorf, D. P. Burdette, J. L. Cozzi, K. B. Howard, S. Zhu, M. P. Carpenter, P. Copp, et al., *Phys. Rev. Lett.* **124**, 052501 (2020).
- [4] S. Nandi, G. Mukherjee, Q. B. Chen, S. Frauendorf, R. Banik, S. Bhattacharya, S. Dar, S. Bhattacharyya, C. Bhattacharya, S. Chatterjee, et al., *Phys. Rev. Lett.* **125**, 132501 (2020).
- [5] P. Bringel, G. B. Hagemann, H. Hübel, A. Al-khatib, P. Bednarczyk, A. Bürger, D. Curien, G. Gangopadhyay, B. Herskind, D. R. Jensen, et al., *Eur. Phys. J. A* **24**, 167 (2005).
- [6] S. W. Ødegård, G. B. Hagemann, D. R. Jensen, M. Bergström, B. Herskind, G. Sletten, S. Törmänen, J. N. Wilson, P. O. Tjøm, I. Hamamoto, et al., *Phys. Rev. Lett.* **86**, 5866 (2001).
- [7] D. R. Jensen, G. B. Hagemann, I. Hamamoto, S. W. Ødegård, B. Herskind, G. Sletten, J. N. Wilson, K. Spohr, H. Hübel, P. Bringel, et al., *Phys. Rev. Lett.* **89**, 142503 (2002).
- [8] G. Schönwaßer, H. Hübel, G. B. Hagemann, P. Bednarczyk, G. Benzoni, A. Bracco, P. Bringel, R. Chapman, D. Curien, J. Domscheit, et al., *Phys. Lett. B* **552**, 9 (2003).
- [9] H. Amro, W. C. Ma, G. B. Hagemann, R. M. Diamond, J. Domscheit, P. Fallon, A. Gorgen, B. Herskind, H. Hübel, D. R. Jensen, et al., *Phys. Lett. B* **553**, 197 (2003).
- [10] D. J. Hartley, R. V. F. Janssens, L. L. Riedinger, M. A. Riley, A. Aguilar, M. P. Carpenter, C. J. Chiara, P. Chowdhury, I. G. Darby, U. Garg, et al., *Phys. Rev. C* **80**, 041304(R) (2009).
- [11] J. T. Matta, U. Garg, W. Li, S. Frauendorf, A. D. Ayangeakaa, D. Patel, K. W. Schlax, R. Palit, S. Saha, J. Sethi, et al., *Phys. Rev. Lett.* **114**, 082501 (2015).
- [12] N. Sensharma, U. Garg, S. Zhu, A. D. Ayangeakaa, S. Frauendorf, W. Li, G. Bhat, J. A. Sheikh, M. P. Carpenter, Q. B. Chen, et al., *Phys. Lett. B* **792**, 170 (2019).
- [13] S. Biswas, R. Palit, S. Frauendorf, U. Garg, W. Li, G. H. Bhat, J. A. Sheikh, J. Sethi, S. Saha, P. Singh, et al., *Eur. Phys. J. A* **55**, 159 (2019).
- [14] C. M. Petrache, P. M. Walker, S. Guo, Q. B. Chen, S. Frauendorf, Y. X. Liu, R. A. Wyss, D. Mengoni, Y. H. Qiang, A. Astier, et al., *Phys. Lett. B* **795**, 241 (2019).
- [15] Q. B. Chen, S. Frauendorf, and C. M. Petrache, *Phys. Rev. C* **100**, 061301(R) (2019).
- [16] S. Chakraborty, H. P. Sharma, S. S. Tiwary, C. Majumder, A. K. Gupta, P. Banerjee, S. Ganguly, S. Rai, Pragati, Mayank, et al., *Phys. Lett. B* **811**, 135854 (2020).
- [17] J. Timár, Q. B. Chen, B. Kruzsicz, D. Sohler, I. Kuti, S. Q. Zhang, J. Meng, P. Joshi, R. Wadsworth, K. Starosta, et al., *Phys. Rev. Lett.* **122**, 062501 (2019).
- [18] M. S. R. Laskar, R. Palit, S. N. Mishra, N. Shimizu, Y. Utsuno, E. Ideguchi, U. Garg, S. Biswas, F. S. Babra, R. Gala, et al., *Phys. Rev. C* **101**, 034315 (2020).
- [19] Q. B. Chen, S. Frauendorf, N. Kaiser, U.-G. Meißner, and J. Meng, *Phys. Lett. B* **807**, 135596 (2020).
- [20] I. Hamamoto, *Phys. Rev. C* **65**, 044305 (2002).
- [21] I. Hamamoto and B. R. Mottelson, *Phys. Rev. C* **68**, 034312 (2003).
- [22] W. X. Shi and Q. B. Chen, *Chin. Phys. C* **39**, 054105 (2015).
- [23] E. Streck, Q. B. Chen, N. Kaiser, and U.-G. Meißner, *Phys. Rev. C* **98**, 044314 (2018).
- [24] R. Budaca, *Phys. Rev. C* **97**, 024302 (2018).
- [25] Q. B. Chen, N. Kaiser, U.-G. Meißner, and J. Meng, arXiv: **nucl-th**, 2003.04065 (2020).
- [26] B. Qi, H. Zhang, S. Y. Wang, and Q. B. Chen, arXiv: **nucl-th**, 2009.05911 (2020).
- [27] Q. B. Chen and S. Frauendorf, arXiv: **nucl-th**, 2012.03499 (2020).
- [28] Q. B. Chen, N. Kaiser, U.-G. Meißner, and J. Meng, *Phys. Lett. B* **807**, 135568 (2020).
- [29] Y. R. Shimizu and M. Matsuzaki, *Nucl. Phys. A* **588**, 559 (1995).
- [30] M. Matsuzaki, Y. R. Shimizu, and K. Matsuyanagi, *Phys. Rev. C* **65**, 041303 (2002).
- [31] Y. R. Shimizu, T. Shoji, and M. Matsuzaki, *Phys. Rev. C* **77**, 024319 (2008).
- [32] S. Frauendorf and F. Dönau, *Phys. Rev. C* **92**, 064306 (2015).
- [33] Q. B. Chen, S. Q. Zhang, P. W. Zhao, and J. Meng, *Phys. Rev. C* **90**, 044306 (2014).
- [34] Q. B. Chen, S. Q. Zhang, and J. Meng, *Phys. Rev. C* **94**, 054308 (2016).
- [35] J. A. Sheikh, G. H. Bhat, W. A. Dar, S. Jehangir, and P. A. Ganai, *Phys. Scr.* **91**, 063015 (2016).
- [36] M. Shimada, Y. Fujioka, S. Tagami, and Y. R. Shimizu, *Phys. Rev. C* **97**, 024319 (2018).
- [37] Y. K. Wang, F. Q. Chen, and P. W. Zhao, *Phys. Lett. B* **802**, 135246 (2020).